The endocytic protein GRAF1 is directed to cell-matrix adhesion sites and regulates cell spreading

Gary J. Doherty[a,*], Monika K. Åhlund[b,*], Mark T. Howes[c], Björn Morén[b], Robert G. Parton[c], Harvey T. McMahon[a], and Richard Lundmark[b]

[a]MRC Laboratory of Molecular Biology, Cambridge CB2 0QH, United Kingdom; [b]Medical Biochemistry and Biophysics, Umeå University, 901 87 Umeå, Sweden; [c]Institute for Molecular Bioscience and Centre for Microscopy and Microanalysis, University of Queensland, Brisbane QLD 4072, Australia

ABSTRACT **The rho GTPase-activating protein GTPase regulator associated with focal adhesion kinase-1 (GRAF1) remodels membranes into tubulovesicular clathrin-independent carriers (CLICs) mediating lipid-anchored receptor endocytosis. However, the cell biological functions of this highly prevalent endocytic pathway are unclear. In this article, we present biochemical and cell biological evidence that GRAF1 interacted with a network of endocytic and adhesion proteins and was found enriched at podosome-like adhesions and src-induced podosomes. We further demonstrate that these sites comprise microdomains of highly ordered lipid enriched in GRAF1 endocytic cargo. GRAF1 activity was upregulated in spreading cells and uptake via CLICs was concentrated at the leading edge of migrating cells. Depletion of GRAF1, which inhibits CLIC generation, resulted in profound defects in cell spreading and migration. We propose that GRAF1 remodels membrane microdomains at adhesion sites into endocytic carriers, facilitating membrane turnover during cell morphological changes.**

Monitoring Editor
Yu-Li Wang
Carnegie Mellon University

Received: Dec 2, 2010
Revised: Aug 16, 2011
Accepted: Sep 20, 2011

INTRODUCTION

Cells interact with their immediate environments through the ligation of plasma membrane-anchored or transmembrane receptors for soluble molecules, such as growth factors, extracellular matrix components, and proteins presented on the surface of neighboring cells. Cell-matrix adhesions are local, dynamic attachments of cell-surface proteins, including integrins and glycophosphatidylinositol-anchored proteins (GPI-APs), to extracellular matrix components that allow indirect bridging of this matrix to the internal cytoskeleton. These dynamic anchor points determine the position of the cell in space and allow cells to undergo shape changes, including those required during cell division, spreading, and migration (Doherty and McMahon, 2008). Initial sites of such adhesion can produce focal complexes, which can 1) be disassembled (if conditions so dictate); 2) become stabilized; or 3) grow into larger, more mature (and less dynamic) adhesion sites, known as focal adhesions, that allow strong connection of the matrix to actin stress fibers. The diversity and dynamics of these integrin-based adhesions, including podosomes and invadopodia, are coordinated by the activity of rho-family small G proteins that transduce internal and external cues into signals for the development, maintenance, growth, and disassembly of these anchor points.

The turnover of adhesion-associated lipid domains and proteins has the potential to regulate adhesion sites, and several studies have suggested an important role for endocytosis in their dynamics (reviewed in Caswell *et al*. [2009]). Adhesive sites strongly affect lipid order and promote the formation of microdomains necessary for certain endocytic events. Interestingly, loss of adhesion correlates with rapid endocytosis of molecules enriched in microdomains, such as cholera toxin B subunit (CTxB; del Pozo *et al*., 2004; Schlunck *et al*., 2004; Gaus *et al*., 2006). It has been shown that focal adhesion

This article was published online ahead of print in MBoC in Press (http://www.molbiolcell.org/cgi/doi/10.1091/mbc.E10-12-0936) on September 30, 2011.

*These authors contributed equally to this work.

The authors declare no competing interests.

Address correspondence to: Richard Lundmark (Richard.lundmark@medchem.umu.se).

Abbreviations used: BAR, Bin/amphiphysin/Rvs; CLIC, clathrin-independent carrier; CTxB, cholera toxin B subunit; DA, dominant-active; DTT, dithiothreitol; FAK, focal adhesion kinase; GFP, green fluorescent protein; GIT1, G protein–coupled receptor kinase–interacting ArfGAP 1; GPI-AP, glycophosphatidylinositol-anchored protein; GRAF1, GTPase regulator associated with focal adhesion kinase-1; GST, glutathione *S*-transferase; MEF, mouse embryonic fibroblast; PBS, phosphate-buffered saline; pFAK, phosphorylated FAK; PH, pleckstrin homology; PIP2, phosphatidyl inositol 4,5 bisphosphate; PLA, podosome-like adhesion; RFP, red fluorescent protein; rhoGAP, rho GTPase-activating protein; ROCK, rho kinase; siRNA, small interfering RNA; Tfn, transferrin.

turnover can be induced by regrowth of microtubules after their depolymerization in a process that requires the endocytic protein dynamin and focal adhesion kinase (FAK; Ezratty *et al.*, 2005, 2009). Dynamin is also found at podosomes. These are rather small and highly active adhesion sites comprising adhesion proteins with an actin core. Here, dynamin is thought to function in the interplay between membrane and actin dynamics (Ochoa *et al.*, 2000).

The best understood endocytic process is mediated by the coat protein clathrin, but cells use a variety of alternative, clathrin-independent endocytic routes (Doherty and McMahon, 2009). The most prevalent of these in fibroblasts is mediated by clathrin-independent carriers (CLICs; reviewed in Mayor and Pagano [2007]; Hansen and Nichols [2009]; Howes *et al.* [2010b]). We have recently shown that the membrane remodeling protein GTPase regulator associated with focal adhesion kinase-1 (GRAF1) regulates GPI-APs and CTxB uptake into CLICs, as well as a large proportion of fluid-phase uptake (Lundmark *et al.*, 2008). These pleiomorphic, tubulovesicular carriers lack an obvious protein coat and form in the absence of clathrin and caveolin (Kirkham *et al.*, 2005). Internalization of GPI-APs and other microdomain-enriched molecules via these carriers depends upon the activity of cdc42, GRAF1, Arf1, ordered lipid microdomains, and actin polymerization (Sabharanjak *et al.*, 2002; Chadda *et al.*, 2007; Kumari and Mayor, 2008; Lundmark *et al.*, 2008). GRAF1 has a rho GTPase-activating protein (rhoGAP) domain that stimulates the GTPase activity of cdc42 in vitro (Hildebrand *et al.*, 1996), as well as Bin/amphiphysin/Rvs (BAR) and pleckstrin homology (PH) domains required for membrane binding and CLIC formation. We describe a link between the endocytic activity of GRAF1 and adhesion modulation. GRAF1 was found enriched at podosome-like adhesions induced in HeLa cells. Our investigations of the activity of these structures support a central role for GRAF1 and CLIC production in cell spreading and migration through modulation of the dynamics of these adhesion sites.

RESULTS

The GRAF1 interactome links endocytosis and cell adhesion

Monomers of the dimeric protein GRAF1 are composed of BAR, PH, rhoGAP, and SH3 domains (Figure 1A). Our previous studies have shown that GRAF1 is necessary for the generation of clathrin-independent endocytic carriers that endocytose a large amount of extracellular fluid and cargoes that include CTxB and GPI-APs (Lundmark *et al.*, 2008). GRAF1 has also been implicated in regulation of focal adhesions and cytoskeletal rearrangements (Hildebrand *et al.*, 1996). To address how these seemingly distinct roles might be linked, we first sought to identify additional proteins that function together with GRAF1. We immunoprecipitated GRAF1 from rat brain cytosol and identified dynamin, FAK, and G protein–coupled receptor kinase–interacting ArfGAP 1 (GIT1) as interacting partners using mass spectrometry and immunoblotting (Figure 1B). We also tested whether GRAF1 could be isolated by immunoprecipitating dynamin, FAK, or GIT1. Under these conditions, GRAF1 coimmunoprecipitated with dynamin, but not with either FAK or GIT1, suggesting that these interactions were weaker or that the antibodies perturbed the binding (Figure 1C, top panel). GRAF1 could, however, be coimmunoprecipitated with the active, phosphorylated form of FAK, pFAK (Figure 1C, bottom panel). Pulldown studies using the GRAF1 SH3 domain as bait in rat brain cytosol verified that the interaction to dynamin and FAK was dependent on this domain (Figure 1D). We then showed that GRAF1, GIT1, and dynamin are found together at a subset of basal plasma membrane structures in HeLa cells, suggesting that GRAF1 also interacts with these proteins in vivo (Figure 1E). GIT1 is an Arf GTPase-activating protein that localizes to cell-matrix adhesions; it has been proposed that GIT1 promotes adhesion down-regulation and cell spreading (Zhao *et al.*, 2000; Manabe *et al.*, 2002) and influences endocytosis and recycling of G protein–coupled receptors (Premont *et al.*, 1998; Claing *et al.*, 2000; Lahuna *et al.*, 2005). Interestingly, the endocytic membrane fission protein dynamin is also implicated in cell-matrix adhesion site turnover and is present at podosomes and focal complexes (Ochoa *et al.*, 2000; Ezratty *et al.*, 2005). The known interactions of GRAF1 are illustrated in an interactome in Figure 1F. Taken together with previous results, our observations suggest that the N-terminal BAR and PH domains endow GRAF1 with the ability to generate/stabilize highly curved endocytic membranes from ordered, phosphatidyl inositol 4,5-bisphosphate (PIP2)-enriched plasma membrane regions, while the C-terminal rhoGAP and SH3 domains modulate rho-family small G-protein activity and interact with dynamin and FAK.

GRAF1 is not a general component of focal adhesions but localizes to podosome-like adhesions

Given the nature of the GRAF1 interactome, we examined whether GRAF1 localization/function was linked to adhesion sites. When GRAF1 was expressed at very high levels, cells underwent a drastic morphological rearrangement, developing long protrusions and collapsing around the nucleus (Taylor *et al.*, 1999; Supplemental Figure S1, A and B). In these cells, the typical focal adhesions and actin stress fibers seen in low-level, overexpressing cells or control cells were absent, and only a few, small punctate adhesions containing vinculin and actin could be detected. When cells with endogenous or low levels of overexpressed GRAF1 were costained with markers for adhesions such as vinculin, we found that GRAF1 was not detected at large, elongated adhesions known as mature focal adhesions (see Figure S1, C and D). Instead, both endogenous and overexpressed GRAF1 were found enriched at small, round, vinculin-positive structures in a subset of cells (see Figure S1, C and D). Our data suggested that GRAF1 might be recruited to a specific intermediate state of adhesive structures. To determine whether its interacting partner GIT1, which is normally found at cell-matrix adhesion sites, could promote the localization of GRAF1 to adhesion sites, we co-overexpressed these proteins. This resulted in fewer mature focal adhesions and a large increase in the number of vinculin- and GRAF1-positive structures (Figure 2, A and B). This is consistent with previous observations that GIT1 promotes turnover of focal adhesions (Zhao *et al.*, 2000) and promotes podosome formation (Wang *et al.*, 2009).

GRAF1-positive adhesive structures closely resembled podosome-like adhesions (PLAs) previously described to be induced by expression of dominant-active cdc42 in HeLa cells (Dutartre *et al.*, 1996). Therefore, to further verify that GRAF1 localized to cdc42-induced adhesions, we coexpressed dominant active cdc42 (cdc42 Q61L; herein named cdc42-DA) with GRAF1 and costained these cells for vinculin. Indeed, we found that co-overexpressing cells exhibited GRAF1 in cdc42- and vinculin-positive PLAs (Figure 2C). Interestingly, these structures were found to contain punctate actin and dynamin, consistent with their similarity to podosomes and the fact that dynamin has a role at adhesions (see Figure S1, E and F). To verify that it is prolonged local cdc42 activity that promotes adhesion localization of GRAF1, we expressed the GRAF1 arginine finger mutant, GRAF1 R412D, in cells. This mutant, which is incapable of stimulating GTP hydrolysis by cdc42, significantly increased the proportion of cells with abundant PLAs containing both vinculin and GRAF1 (Figures 2B and S1G). The R412D mutation

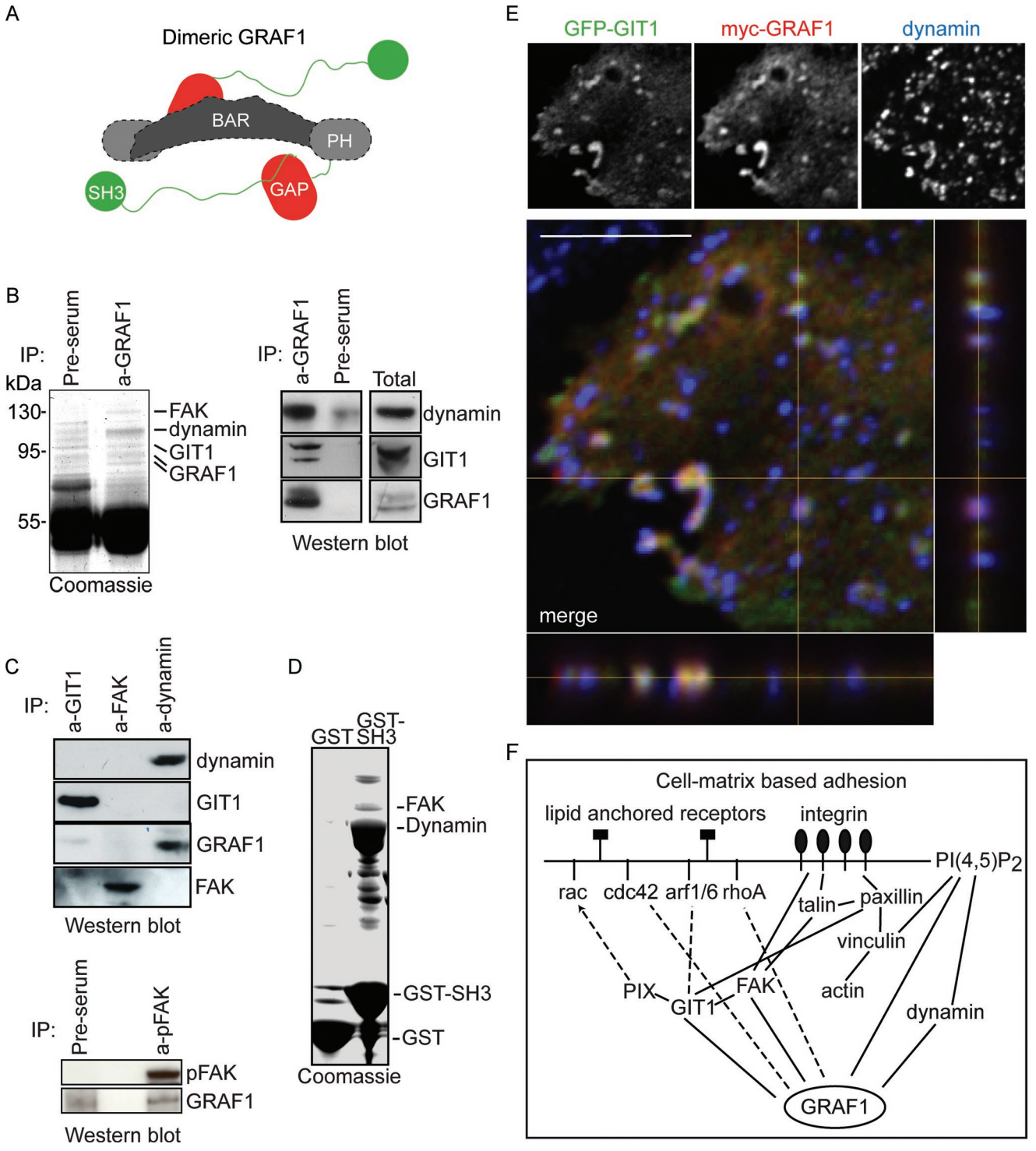

FIGURE 1: GRAF1 interacts with proteins involved in membrane remodeling and cell adhesion. (A) Domain model of GRAF1. (B) Immunoprecipitation of GRAF1 from rat brain cytosol showing that GRAF1 interacts with dynamin, GIT1, and FAK as identified by mass spectrometry and confirmed by Western blotting with the indicated antibodies. (C) Immunoprecipitates of GIT1, FAK, dynamin, and pFAK from rat brain cytosol were analyzed by SDS–PAGE and immunoblotting with antibodies against the indicated proteins. (D) Coomassie-stained gel of pulldown experiments against brain lysates with beads bound to GST or GST-tagged GRAF1 SH3 domain (GST-SH3). Indicated proteins were identified by mass spectrometry. (E) Confocal micrograph of a HeLa cell expressing GFP-GIT1 and myc-GRAF1, costained for dynamin. Merged image shows section views (as indicated by yellow lines). Note that structures with all three proteins colocalizing are found at the basal surface, while dynamin is also found at the top surface. Scale bar: 5 μm. (F) Schematic representation of the GRAF1 interactome, showing the interactions that link cell adhesion, small G-protein regulation, and GRAF1-mediated membrane trafficking (Hildebrand *et al.*, 1996; Zamir and Geiger, 2001a, 2001b; Hoefen and Berk, 2006; Lundmark *et al.*, 2008). Dotted lines show interactions known to be directly activating (arrowheads) or inhibiting (no arrowheads) the active state of depicted small G protein.

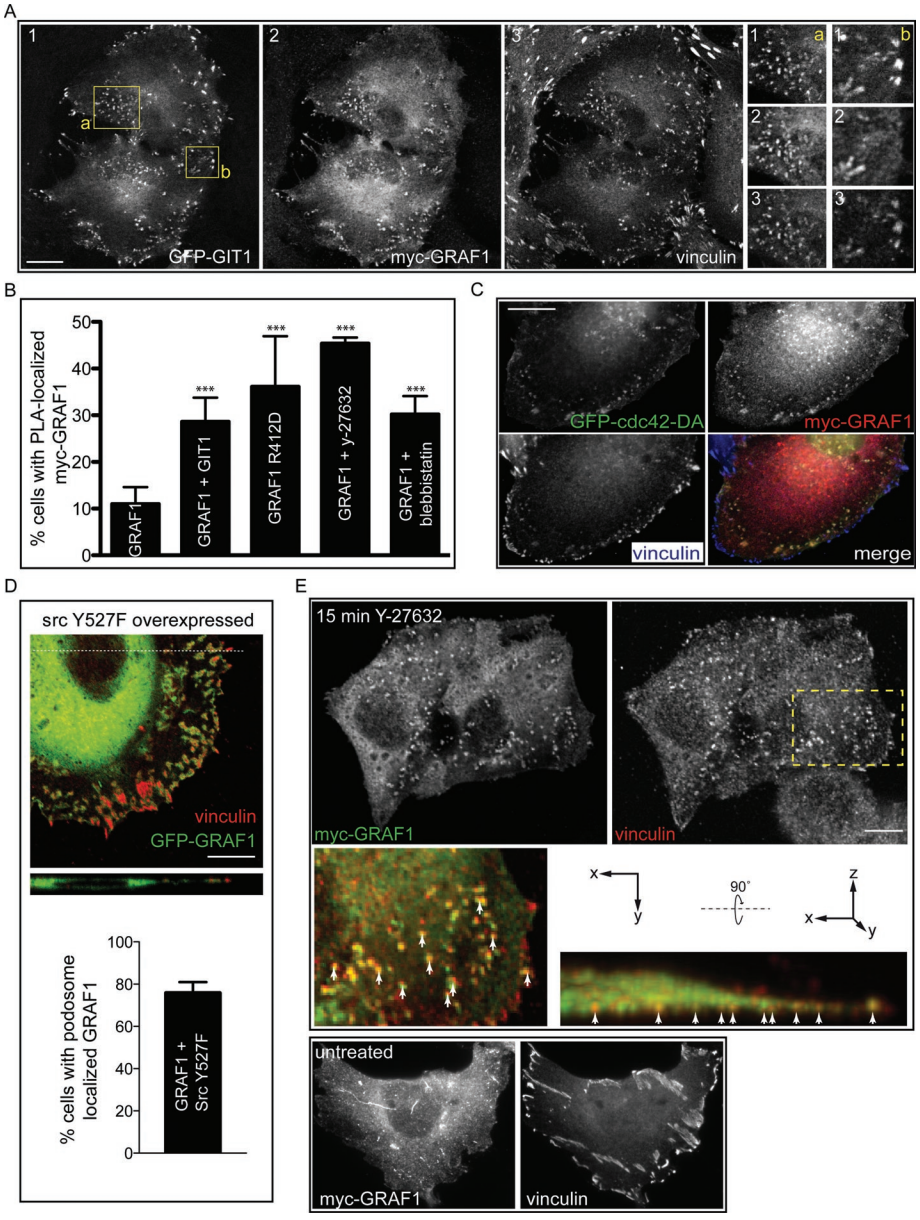

FIGURE 2: GRAF1 is not a general component of focal adhesions but localizes to PLAs. (A) Fluorescence micrograph of HeLa cells coexpressing myc-tagged GRAF1 and GFP-tagged GIT1 and costained for myc and vinculin. Insets show magnifications of the areas indicated by yellow squares. (B) Bar graph showing the percentage of cells in which myc-GRAF1 or myc-GRAF1 R412D was found localized with vinculin in PLAs following the indicated treatments or overexpression of GFP-GIT1. Cells expressing myc-GRAF1 were treated with Y-27632, an inhibitor of rhoA kinase (5 min), or blebbistatin, an inhibitor of nonmuscle myosin II (10 min), and the number of cells where GRAF1 colocalized with vinculin was counted. Bars and error bars correspond to mean and SEM calculated from three independent experiments ($n > 250$; $\alpha = 0.05$; two-tailed Fisher's exact test, ***, $p < 0.001$). (C) Fluorescence micrograph of cells coexpressing myc-tagged GRAF1 and GFP-cdc42-DA and costained for myc and vinculin. (D) Merged confocal micrograph of a cell expressing src Y527F and GFP-GRAF1 and costained for vinculin. Inset below shows three-dimensional view of the section indicated by the dotted line. Bar graph depicting the percentage of cells with untagged or GFP-tagged GRAF1 localized to vinculin-defined, src-induced podosomes. Bars and error bars correspond to mean and SEM calculated from six independent experiments, each including 30 cells. (E) Fluorescence micrographs of cells treated with the ROCK inhibitor Y-27632 for 15 min or untreated before fixation and staining for vinculin and overexpressed myc-GRAF1. Insets in the top panel show magnification and three-dimensional rotation of the area indicated in the vinculin panel. Arrows indicate basal structures in which GRAF1 and vinculin colocalize. Scale bars: 10 μm.

also significantly abrogated GRAF1's ability to cause profound cellular morphological changes (Figure S1B).

GRAF1 localizes to src-induced podosomes

Podosome formation is highly stimulated by src kinase through activation of cdc42, and active src has been used to promote podosome formation in a number of cell lines (Moreau *et al.*, 2006). To assay whether src-induced podosomes contained GRAF1, we expressed the dominant active version of src (src Y527F) in HeLa cells. This clearly induced both small and rosette-like basal adhesions that, similarly to podosomes, were positive for vinculin, cortactin, and pFAK (Figures 2D and S2). When costained for GRAF1, the majority (76%) of cells with such podosomes were found to have GRAF1 highly enriched in these structures (Figure 2D). These results verified the similarity between podosomes and GRAF1-positive adhesive structures and indicated that GRAF1 might have a role at bona fide podosomes. On the basis of size and appearance; the presence of dynamin, punctate actin, and cortactin; and the dependence on cdc42 and src activity, we propose that GRAF1 is present at a subset of adhesions most accurately described to date as PLAs.

Acute adhesion site modulation by small molecules results in clustering of CTxB in GRAF1-positive PLAs

Cell-matrix adhesions are dependent upon the contractive force mediated by myosin and actin filaments. This process is controlled by cdc42, rhoA, and rac1, and induction of PLAs is thought to rely upon cdc42 activity (Nobes and Hall, 1995; Moreau *et al.*, 2006). To favor cdc42 activity over rhoA activity acutely, we inhibited the rhoA effector protein rho kinase (ROCK), a key regulator of adhesions (Totsukawa *et al.*, 2000). Inhibition of ROCK using the small molecule Y-27632 led to a dramatic loss of actin stress fibers and focal adhesions in favor of PLAs (Figure S3A). In GRAF1-expressing cells, we observed a profound increase in the proportion of cells exhibiting PLA-localized GRAF1 on their basal surfaces (Figures 2, B and E, and S3, B–D). Similarly, the drug blebbistatin, which induces loss of stress fibers, resulted in a significantly increased number of PLAs positive for GRAF1 (Figures 2B and S3E).

The membrane at cell-matrix adhesions is composed of highly ordered lipids that are also necessary for endocytosis via CLICs

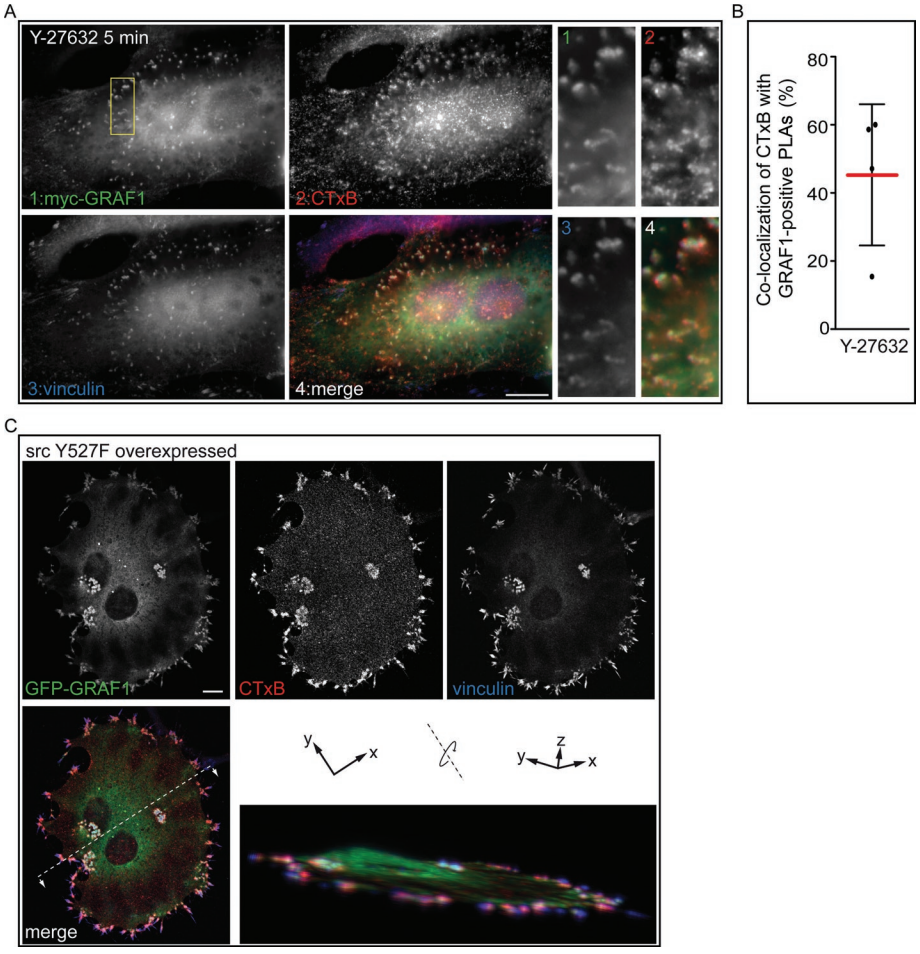

FIGURE 3: Adhesion reorganization results in clustering of CTxB at the cell surface in GRAF1-positive structures. (A) Fluorescence micrographs of myc-GRAF1–expressing HeLa cells incubated with Y-27632 together with CTxB-Alexa555 for 5 min as indicated before washing, fixation, and costaining for vinculin. Insets are magnifications of the area marked by a rectangle in panel 1. (B) Vinculin- and myc-GRAF1-positive PLA areas were selected from four cells from two different experiments, and the percent colocalization of CTxB was measured as described in the text. The mean is indicated by a red line and the error bars represent standard deviation (SD) above and below the mean. (C) Confocal micrograph of cell expressing src Y527F and GFP-GRAF1 and incubated together with CTxB-Alexa555 for 5 min before washing, fixation, and costaining for vinculin. The merged image is rotated to highlight the basal localization of GRAF1-positive structures. Scale bars; 10 μm.

(Sims and Dustin, 2002; Gaus *et al.*, 2006). We therefore examined whether induced PLAs and podosomes contained the GM1 receptor, a glycosphingolipid that is enriched in microdomains. When CTxB, which binds GM1 specifically, was added to Y-27632-treated cells, we found that it clustered in vinculin-positive structures on the membrane, overlapping closely with GRAF1 localization (Figure 3A). Treatment with blebbistatin likewise resulted in clustering of CTxB at PLAs containing GRAF1 (Supplemental Figure S3E). We measured the amount of colocalization and found that approximately one-half the area of acutely induced PLAs contained CTxB (Figure 3B). Our data show that acute induction of adhesion turnover affects membrane order and GRAF1 activity, which supports the view that plasma membrane dynamics are closely coupled to cell-matrix adhesion turnover. The presence of GRAF1 at src-induced podosomes indicates that these structures might have a similar membrane composition. Indeed, we found that CTxB was clustered in src-induced podosomes together with GRAF1 (Figure 3C).

Membrane remodeling by GRAF1 and uptake of CTxB is stimulated at the leading edge of migrating cells

As previously shown (Lundmark *et al.*, 2008), CTxB was internalized by tubular GRAF1-positive structures (Figure 4A). We observed that these structures communicated with adhesion sites, supporting a role for GRAF1 in promoting endocytosis of lipids enriched in sites of high membrane order (Figure 4A). Similarly, the long, "trapped" membrane tubules generated by the overexpression of GRAF1 BARPH truncation mutant (Lundmark *et al.*, 2008) spanned long stretches along the basal surface of cells, linking mature focal adhesions (Figure S4C). When tracked by live-cell imaging, the formation of GRAF1 R412D- and GRAF1 BARPH-positive tubules (which are more stable then GRAF1-positive tubules) was detected. These tubules were found to both originate from, and specifically communicate with, sites of adhesions (Figure S4 and Supplemental Movies S1–S4). This suggested that GRAF1-mediated membrane trafficking is coupled to adhesion modulation. To study how GRAF1-mediated and clathrin-dependent endocytic events are influenced by the movement of cells, we examined the uptake of the CLIC cargo CTxB and the clathrin-mediated endocytosis cargo transferrin (Tfn) by migrating fibroblasts (which are more migratory than HeLa cells; Figure 4B). We found that the uptake of CTxB was concentrated at the leading edge of the cell. By contrast, Tfn, a clathrin-dependent endocytic cargo, appeared to be endocytosed homogeneously from the plasma membrane, consistent with previous studies (Howes *et al.*, 2010a). Furthermore, CTxB-enriched endocytic structures were found to colocalize with paxillin, a marker of integrin-based adhesions, to a significantly higher extent than with Tfn (Figure 4C).

Given these data, one might therefore expect that GRAF1-mediated endocytic activity would be affected by adhesion and spreading of cells. Rac1 promotes cell spreading and lamellopodia/ruffles at the leading edges of cells (Nobes and Hall, 1995). We therefore examined whether rac1-induced cell spreading could also induce GRAF1-mediated endocytosis. Cells expressing dominant-active rac1 (rac1 Q61L; herein named rac1-DA) had a round, spread-out morphological phenotype with prevalent ruffled structures containing rac1. Strikingly, when GRAF1 was co-overexpressed in these cells, we found it on large numbers of membrane tubules at the ruffled regions (Figure 4D and Movie S5). These tubular structures contained CTxB (Figure 4D, right panel). In contrast with both cdc42 and rac1, rhoA activity is known to promote cell adhesion and contraction. Expression of DA rhoA (rhoA Q63L; herein named rhoA-DA) results in the rounding up of cells and promotion of mature focal adhesions. Co-overexpression of rhoA-DA and GRAF1 likewise led to contracted cells (owing to actin stress fiber formation and maintenance; Figure 4E). GRAF1-positive tubular structures

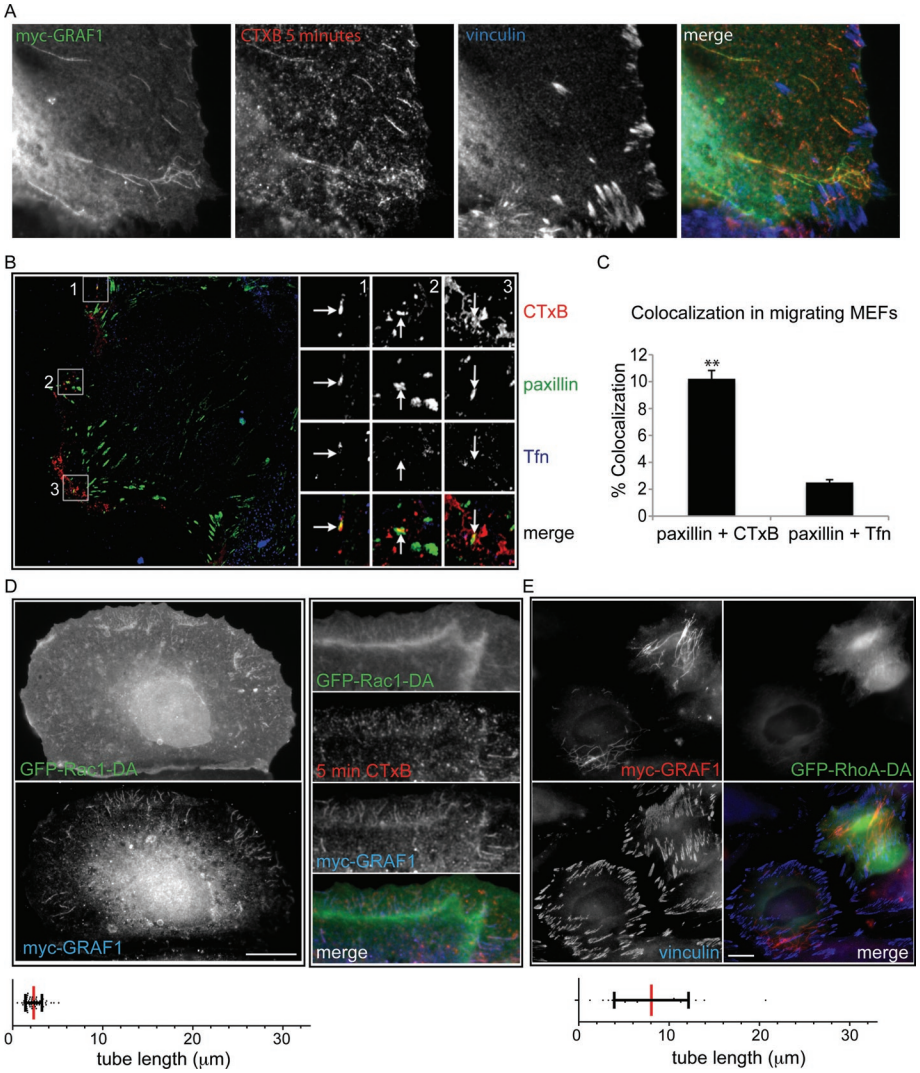

FIGURE 4: Membrane remodeling by GRAF1 and uptake of CTxB are stimulated at the leading edge of migrating cells. (A) Fluorescence micrographs of myc-GRAF1–expressing HeLa cells incubated with CTxB-Alexa555 for 5 min before washing, fixation, and costaining for vinculin. (B) Confluent wild-type MEF monolayers were wounded by scratching, and cells were allowed to migrate into the wound for 4–6 h. CTxB-555 and Tfn-647 were then added to migrating cells for 2 min of uptake at 37°C. Cells were acid-stripped and fixed and were then labeled for endogenous paxillin. Arrows indicate colocalization between paxillin and CTxB but not Tfn. (C) Twenty-four cells across three independent experiments were treated as in (B), and the percentage of paxillin (green) pixels that colocalized with either CTxB (red) or Tfn (blue) pixels was calculated using Volocity version 3.0. Bars and error bars correspond to mean and SEM ($n = 12–15$; $\alpha = 0.05$; Student's t test, **, $p < 0.01$). (D) Fluorescence micrographs of HeLa cells expressing myc-GRAF1 and DA rac1 (GFP-Rac-DA; left panels) and incubated with CTxB-Alexa555 for 5 min (right panels). The length of GRAF1 tubules was measured in fluorescence micrographs of seven different cells ($n = 193$) as described. The mean length is indicated by a red line and the error bars represent standard deviation (SD) above and below the mean. (E) Fluorescence micrographs of cells expressing myc-GRAF1 and DA rhoA (GFP-rhoA-DA) and costained for vinculin. GRAF1-positive tubules were found in 14.3 ± 3.7%, as determined from three independent experiments ($n = 124$; error values represent SEM). Length of GRAF1 tubules in μm was measured from nine different cells ($n = 108$) and depicted as in Figure 4D. Scale bars: 10 μm.

were found only in a small subset of rhoA-DA–expressing cells (14.3 ± 3.7%). These tubules were much longer than GRAF1-positive tubules in rac1-expressing cells and communicated with focal adhesions (Figure 4E). However, GRAF1 was not enriched at the abundant, mature focal adhesions in rhoA-DA–expressing cells. The tubular phenotype was strikingly reminiscent of that observed upon overexpression of the dominant-negative GRAF1 variant GRAF1 BARPH (Lundmark *et al.*, 2008), suggesting that the associated membrane trafficking is similarly abrogated.

GRAF1 is necessary for efficient spreading and migration of HeLa cells

To determine whether GRAF1 activity was necessary for spreading and migration of cells, we depleted cells of GRAF1 using small interfering RNAs (siRNAs) previously shown to profoundly abrogate CLIC/endocytic membrane manufacture (Lundmark *et al.*, 2008). Immunoprecipitation of GRAF1 from cell lysates and detection by immunoblotting showed that GRAF1 was efficiently depleted using either of two different siRNAs (Figure 5A). When cells were seeded sparsely and allowed to spread after deattachment, we noted that GRAF1-depleted cells were elongated and unable to spread fully, in contrast with validated controls (Figure 5B). We measured the area of experimental cells and found that GRAF1-depleted cells had significantly smaller surface-connected areas compared with control cells. We also found that cells lacking GRAF1 had approximately double the average length:width ratios of controls (Figure 5C). Interestingly, cells lacking rac1 and rac2 displayed a similar elongated phenotype (Wheeler *et al.*, 2006). Two large-scale siRNA screens have identified the gene encoding GRAF1 as being involved in migration and adhesion (Simpson *et al.*, 2008; Winograd-Katz *et al.*, 2009). We observed that GRAF1-depleted cells were deficient in migrating into an induced wound in a cell monolayer (Figure 5D), and the distribution of mature focal adhesions was frequently disturbed (Figure 5E). To obtain real-time quantitative data on migration, we assayed the ability of cells to "heal" an electrically induced wound. While control cells closed the wound within 5–6 h, GRAF1-depleted cells were profoundly deficient in their abilities to spread and migrate into this wound (Figure 5F). Taken together, our data demonstrate a role for GRAF1 in cell migration, due to regulation of cell-matrix adhesion sites through endocytic turnover of membranes.

DISCUSSION

The mechanisms by which plasma membrane morphological changes and membrane trafficking are coupled in processes such as cell migration are greatly debated. Many studies have highlighted the importance of specific rho-family, small G proteins in both cytoskeletal dynamics and endocytic events (Mayor and Pagano, 2007; Doherty and McMahon, 2008). Our studies reported here on membrane remodeling and rhoGAP protein GRAF1 have revealed that a prevalent clathrin-independent endocytic pathway is

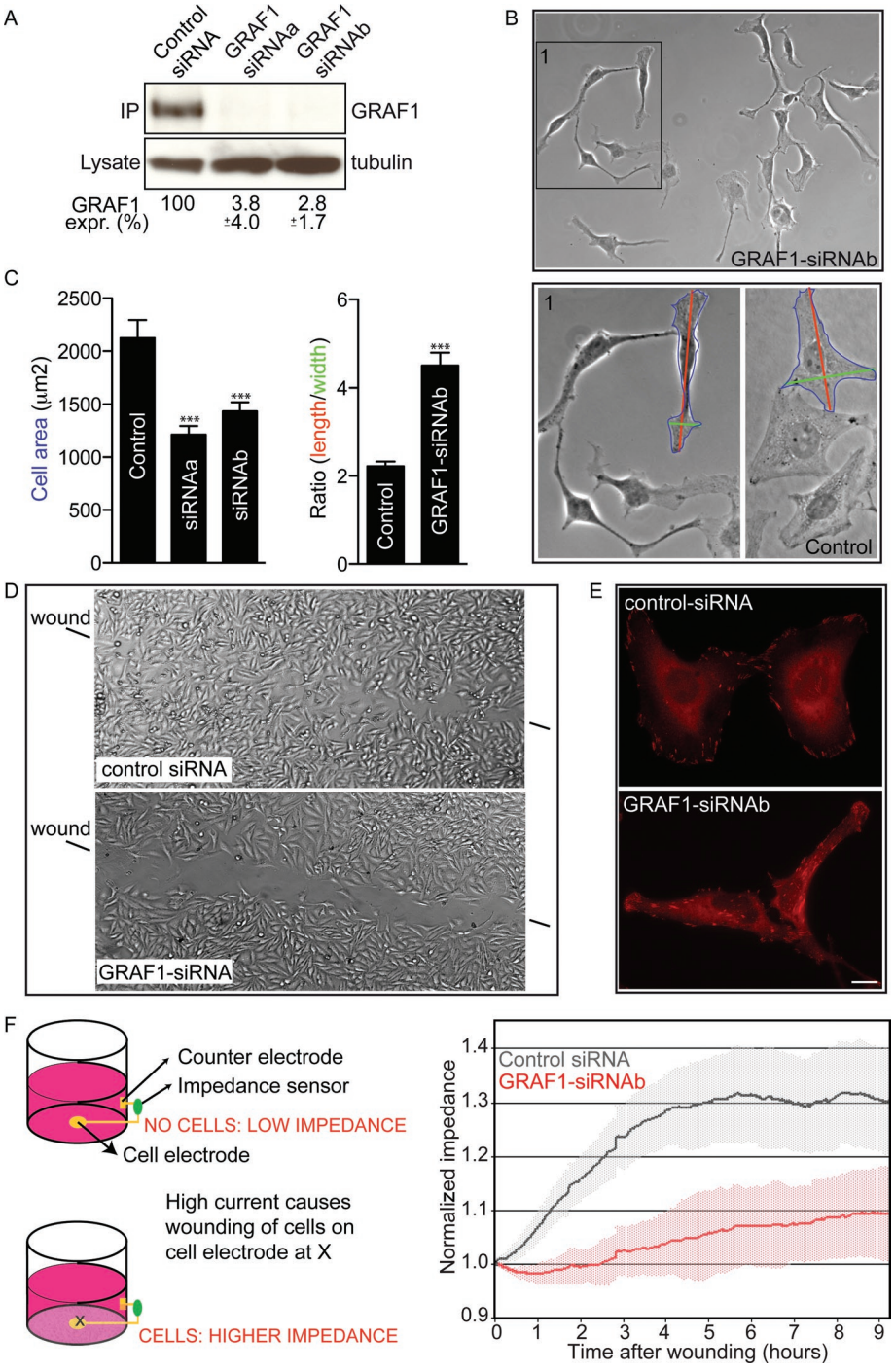

FIGURE 5: GRAF1 is necessary for cell spreading and migration. (A) Immunoprecipitation and immunodetection of GRAF1 from HeLa cells treated with either a control siRNA or siRNAs against GRAF1. Tubulin was detected in the cell lysates as an immunoprecipitation control. GRAF1 expression following siRNA treatment (GRAF1 expr. (%)) was quantified as described from three independent experiments. Values correspond to normalized means ±SD. (B) Micrographs of cells treated with either a control siRNA or siRNAb against GRAF1 for 72 h before fixation and imaging. Inset 1 (left panel) shows magnification of the marked square. Inset 1 (right panel) exemplifies cell area indicated in blue, and length and width indicated in red and green, respectively. (C) Bar graphs showing quantification of the cell area and length:width ratios, as described in the text, of cells treated with control siRNA or siRNAs against GRAF1, as in (B). In the left panel, bars and error bars correspond to mean and SEM calculated from five or six independent experiments (n = 50–60; $\alpha = 0.05$; Student's *t* test, ***, $p < 0.001$). In the right panel, bars and error bars correspond to mean and SEM calculated from two independent experiments (n > 100; a $\alpha = 0.05$; Student's *t* test, ***, $p < 0.001$). Length:width ratio was scored as the ratio between length (longest straight line within a cell (red line in (B)) and width (the broadest region perpendicular to the measured length (green line in (B)). (D) Micrograph showing the regrowth of control siRNA-treated and GRAF1 siRNA-treated cells into an induced wound in the cell monolayer. (E) Fluorescence micrograph of control cells and GRAF1-depleted cells stained for vinculin. (F) Principle of electrically induced and monitored wound-healing assay performed as described (left panel). Graph showing the recovery from electrical wound healing of a confluent HeLa cell layer. Cells were previously transfected with a control siRNA or GRAF1-siRNA, as indicated. An increase in impedance reflects the migration of surrounding healthy cells onto an electrode through which (at time zero) a high current has passed to irreversibly injure the cells on the electrode. Note the delay in wound healing observed in GRAF1-depleted cells and their slowed and incomplete recovery (even after 9 h), compared with control cells. Impedance values were normalized to postwounding nadirs, and the shaded areas surrounding each curve represent one SD above and below the mean values for each condition. Scale bars: 10 µm.

intimately coupled to adhesion site regulation. GRAF1-dependent CLICs are induced by cell spreading, enriched at the leading edge of cells, and necessary for cell spreading and migration. Interestingly, proteomic analysis has recently revealed enrichment for cargo molecules linked to adhesions (Howes *et al.*, 2010a). Although the exact role of GRAF1 in receptor trafficking is not known, our data illuminate an important cell physiological function for GRAF1-dependent CLICs, and provide further insight into how cells coordinate membrane and protein redistribution with changes in their morphologies.

While it has previously been suggested (Hildebrand *et al.*, 1996) that GRAF1 functions at focal adhesions, owing to its interaction with FAK, we find no evidence that GRAF1 is a structural component of such adhesions. However, we found GRAF1 at what, at present, can be best described as PLAs. These structures could be induced by prolonged src and cdc42 activity (through expression of active src, cdc42-DA, or GRAF1 R412D, or by inhibition of ROCK using small molecules) and are enriched in cortactin, actin, dynamin, actin, vinculin, FAK, and GIT1. Although the exact role of GRAF1-positive adhesions is not clear, the localization to src-induced podosomes indicates a relevant function of GRAF1 at such sites. Podosomes are classically found in cells of the monocytic lineage but are becoming increasingly recognized as being present in a number of cell

types. These enigmatic structures are much more dynamic than focal adhesions and resemble the intermediates formed during focal adhesion formation and turnover (Block *et al.*, 2008). Ordinarily, GRAF1-mediated endocytic activity is very dynamic and most prevalent at the leading edge of cells, suggesting that GRAF1-positive PLAs enriched with GM1 might represent a stabilized intermediate that occurs during adhesion turnover (favored by prolonged cdc42 activity or alterations in the integrity of membrane microdomains). Truncated GRAF1, lacking the regulatory GAP and SH3 domains (GRAF1 BARPH), generates long, tubular membrane structures in cells (Lundmark *et al.*, 2008). Interestingly, we found that these tubules frequently spanned long stretches between mature focal adhesions, suggesting that truncated GRAF1 is unable to appropriately regulate the dynamics of membrane carriers at adhesive sites. The real time formation of GRAF1-positive carriers showed that such structures both originate at and are targeted to adhesion sites, suggesting that CLICs might control bidirectional trafficking to regulate membrane turnover.

Our biochemical analyses identified interacting partners of GRAF1 that include FAK, GIT1, and dynamin, supporting a role for GRAF1 at the interface between membrane dynamics and adhesion. Both GIT1 and FAK are known to regulate adhesion sites and influence endocytosis (Premont *et al.*, 1998; Claing *et al.*, 2000). In addition to the established role of dynamin during fission of endocytic carriers, dynamin also localizes to podosomes and invadopodia (Ochoa *et al.*, 2000; Lundmark *et al.*, 2008). Interestingly, a GTPase-deficient mutant of dynamin was found to perturb actin dynamics at such sites (Ochoa *et al.*, 2000; Baldassarre *et al.*, 2003) and a mutant lacking its proline-rich domain (and therefore unable to interact with SH3 domains) was found to disrupt podosome formation (Lee and De Camilli, 2002). Dynamin and GRAF1 interact avidly, with both resulting in plasma membrane invagination. While fission of CLICs from the plasma membrane has been shown to be capable of functioning without dynamin, this does not necessarily mean that all clathrin-independent events are dynamin independent. We show that GRAF1 and dynamin colocalize at PLAs, suggesting that these proteins might organize molecular networks and membrane dynamics at such sites. The membrane architecture at podosomes/PLAs is also presently unclear, but it has been suggested that formation of both podosomes and invadopodia involves membrane invaginations, and our results support this. Uptake of gold-labeled gelatin via narrow membrane tubules has been described as strongly associated with podosome localization, and it has been suggested that dynamin coats membrane tubules in the central region of podosomes (Gawden-Bone *et al.*, 2010; Ochoa *et al.*, 2000). Further ultrastructural studies will assess the precise proteolipid architecture of PLAs, podosomes, and GRAF1-positive tubules and determine whether GRAF1-mediated endocytosis is directly coupled with the internalization of any particular adhesion molecule(s).

Previous work has shown that integrin-based adhesions influence membrane order and control the recruitment of active rac1 to cholesterol-dependent microdomains at the leading edge, where it is found together with the CTxB receptor GM1 (del Pozo *et al.*, 2004; Gaus *et al.*, 2006). Furthermore, detachment of cells from their substrata triggers the internalization of highly ordered regions of the plasma membrane (del Pozo *et al.*, 2004). We show that GRAF1-positive PLAs include highly ordered membranes. CLIC manufacture is likewise dependent upon the presence of highly ordered membranes, and the removal of these lipids from the plasma membrane could promote adhesion turnover through dissipation of adhesion proteins that preferentially accumulate in microdomains. GRAF1-mediated CLIC generation is promoted by rac1 at the leading edge of cells. Indeed, it may be that it is the permissive state of lipids that allows for the spatiotemporal coupling of adhesion site turnover and membrane trafficking. GRAF1 might be recruited to such domains preferentially, owing to both their distinct membrane composition and local, small G-protein activity. The extent of GRAF1-mediated endocytosis linked to adhesion sites versus endocytosis at nonadhesive microdomains appears high, and it appears that this ratio is coordinated with the migratory behavior of the cell. Taken together, our data support a role for GRAF1 at adhesive microdomains, where its membrane remodeling activity promotes the manufacture of CLICs. This activity is promoted at the leading edge of cells, where it is required for membrane spreading and cell migration.

MATERIALS AND METHODS

Reagents, antibodies, and cDNA contructs

Polyclonal antisera against GRAF1 (RA-83 and RaZ1) were generated as previously described (Lundmark *et al.*, 2008). Purchased antibodies were: mouse anti-myc clone 9E10 and rabbit anti-myc (Cell Signaling Technology, Danvers, MA), mouse anti-dynamin (Hudy), mouse anti-GIT1 (BD Biosciences), and mouse anti-paxillin, mouse anti-vinculin, rabbit anti-FAK, rabbit anti-pFAK, and rabbit anti-cortactin (Abcam, Cambridge, MA). All secondary antibodies were conjugated to Alexa Fluor 488, 546, or 647 (Invitrogen, Carlsbad, CA). cDNA constructs encoding human GRAF1 and derivatives were as described previously (Lundmark *et al.*, 2008), except for the amino acid substitution R412D, which was created using PCR-directed mutagenesis (Stratagene, Agilent, Santa Clara, CA). Red fluorescent protein (RFP)-tagged GRAF1 and untagged GRAF1 was cloned using the Gateway system (Invitrogen). Green fluorescent protein (GFP)-tagged cdc42 Q61L (12600; Nalbant *et al.*, 2004), rac1 Q61L (12981), rhoA Q63L (12968; Subauste *et al.*, 2000), and untagged src Y527F (13660) were purchased from Addgene (Cambridge, MA). GFP-GIT1 and RFP-paxillin were kind gifts from A. F. Horwitz and E. E. Marcantonio, respectively. Y-27632 and blebbistatin was purchased from Sigma-Aldrich (St. Louis, MO) and used at 10 and 20 μM, respectively.

Immunoprecipitation and pulldown

For immunoprecipitation experiments, rat brain cytosol was generated by homogenization of rat brains in buffer (25 mM HEPES, 150 mM NaCl, 1 mM dithiothreitol [DTT], 0.1% Triton X-100, and protease inhibitors), before centrifugation at 50,000 rpm for 30 min at 4°C. The supernatant was removed and added to protein A Sepharose 4B beads (GE Healthcare), to which antibodies had been previously bound, and incubated at 4°C for 3 h. Beads were washed three times in buffer (25 mM HEPES, 150 mM NaCl) supplemented with 1% NP-40, and once in buffer without NP-40, before analysis by SDS–PAGE combined with immunoblotting or Coomassie Blue staining. Immunoprecipitation of GRAF1 to determine siRNA efficiency was performed as described above, except that HeLa cells were lysed in buffer (25 mM HEPES, 150 mM NaCl, 1% NP-40, and protease inhibitors), before centrifugation at 14,000 rpm for 30 min at 4°C. Recombinant proteins were expressed in a BL21 (DE3) pLysS *Escherichia coli* strain as glutathione *S*-transferase (GST)-fusion proteins and purified using glutathione-Sepharose 4B beads (Amersham Biosciences) and gel filtration on a sephacryl S-200 column (GE Healthcare). Pulldown experiments against rat brain cytosol using purified proteins and identification by mass spectrometry were performed as previously described (Lundmark *et al.*, 2008).

Cell culture and transfections

HeLa cells and Balb3T3 cells were grown in DMEM media (Gibco, Invitrogen) supplemented with L-glutamine, 10% fetal bovine

serum, and nonessential amino acids (for MEM), and transfected using Lipofectamine 2000 (Invitrogen) or Neon transfection system for electroporation (Invitrogen) for transient protein expression. Mouse embryonic fibroblasts (MEFs) were generated and grown as previously described (Kirkham *et al.*, 2005). For GRAF1 depletion, HeLa cells were transfected with stealth siRNA specific against human GRAF1 (Invitrogen), using Lipofectamine 2000 or Neon transfection system for electroporation according to the manufacturer's instructions. Cells were cultured for 72 h for efficient silencing of the GRAF1 expression. Stealth negative control medium GC Block-it siRNA (Invitrogen) was used as a control. GRAF1 siRNAa: GUA AUCUGUGCUGAAUGGGAGAUAA; GRAF1 siRNAb: CCACUCAUGAUGUACCAGUUUCAAA.

Fixed-sample and real-time imaging

For immunofluorescence analysis, HeLa cells were fixed in 3% paraformaldehyde in phosphate-buffered saline (PBS) for 15 min at 37°C, then washed and blocked in 5% goat serum with 0.05% saponin in PBS before staining with the appropriate antibodies in 1% goat serum with 0.05% saponin in PBS using standard protocols. Confocal images were taken sequentially using either a TCS SP5 system confocal laser-scanning microscope (Leica Microsystems) or a fully motorized A1 R Laser Scanning Confocal Microscope system (Nikon Instruments, USA) using a 60× lens (Plan Apochromat VC Oil DIC N2, Nikon) at appropriate excitation and emission wavelengths under control of the NIS-Elements Microscope Imaging Software. Epifluorescence and phase-contrast images were taken using a Zeiss Axioimager Z1 system with AxioVision software. Images were processed using Adobe Photoshop CS2 (San Jose, CA). For immunofluorescence trafficking assays in HeLa cells, Alexa Fluor 546/555-conjugated CTxB (Invitrogen) was diluted in prewarmed media, added to cells, and incubated for the time periods and temperatures described in the figure legends. After being washed, cells were fixed and subjected to immunofluorescence analysis as described above. For polarized uptake experiments, confluent monolayers of MEFs, grown on 12-mm, round, glass coverslips (Lomb Scientific, Australia) were wounded by scratching with a 200 µl pipette tip. Cells were allowed to migrate into the wound for 4 h before addition of 10 µg/ml CTxB-555 (Invitrogen) and 20 µg/ml Tfn-647 (Invitrogen) for 2 min at 37°C. Cells were fixed in 4% paraformaldehyde and labeled with anti-paxillin antibodies (BD Transduction Laboratories). An axiovert 200 m SP LSM 510 META confocal laser-scanning microscope (Zeiss) was used to capture images, which were processed using Volocity, version 3.7.

Quantification and image analysis

For quantification of the proportion of cells with protrusions, PLA-localized GRAF1, GRAF1 localization to src-induced podosomes, and the length of GRAF1-positive structures, HeLa cells were transfected with constructs for overexpression as indicated in the figure legends and processed for immunofluorescence analysis as described in the preceding section. Protrusive structures (>20 µm long and <10-µm wide protrusions) were measured using Axiovision software (Zeiss), and the proportion of cells with such protrusions was calculated for each condition ($n > 200$ for each condition). The percentage of cells with PLA-localized GRAF1 was counted in three independent experiments for each condition using the Axiovision software ($n > 250$ for each condition). The percentage of cells with src-induced podosomes in which GRAF1 was also localized was calculated from six independent experiments (30 cells per experiment) using the NIS Elements software (Nikon). Length of GRAF1 structures was measured using the ImageJ segmented lines tool. To calculate the length:width ratio of cells, phase-contrast images were captured and the length (longest straight line within a cell) and width (the broadest region perpendicular to the measured length) was measured using ImageJ. For cell area determination, cell borders from 50–60 cells from at least five independent experiments were manually defined in captured phase-contrast images, and the area was calculated using the "Outline" function of the AxioVision software. Creation of bar graphs and statistical analysis was performed using Graphpad Prism (La Jolla, CA). For colocalization experiments in migrating cells, 12–15 cells in three independent experiments were processed using Volocity, version 3.7, and colocalization was determined using the colocalization function with automatic threshold. Automatic thresholds were applied to individual cells, and percentage of overlapping pixels was calculated for CTxB and Tfn channels against paxillin. For quantification of the colocalization between CTxB and PLAs, 3–10 separate images of each condition were thresholded for the brightest areas; overlapping areas were then transferred into a new channel. GRAF1- and vinculin-positive PLA areas were manually defined, and the amount of CTxB colocalization in these areas was calculated using Adobe Photoshop. For determining the amount of GRAF1 following siRNA treatment, intensity of GRAF1 and tubulin bands identified by immunoblotting from three independent experiments was quantified using ImageJ. GRAF1 intensity was related to tubulin intensity for each sample, and the amount of GRAF1 in control cells was set to 100%.

Biophysical cell recordings

HeLa cells (10^5) were transfected with siRNA against GRAF1 or control siRNA for 24 h before being plated into chambers of 8W1E electrode arrays (Applied Biophysics, Troy, NY) and incubated at 37°C with 5% CO_2. Impedance values between the electrode and counterelectrode were recorded continuously from each array at a 15-kHz oscillator frequency using an ECIS 1600 system with elevated field module (Electric Cell-substrate Impedance Sensing, Applied Biophysics). Cell attachment, spreading, and layer confluence were verified electrically and microscopically before electrical wounding at 45 kHz, 4 V for 10 s with subsequent recording from electrodes using the same parameters as prewounding. Data were normalized to initial electrode impedance value for each wounding experiment.

ACKNOWLEDGMENTS

This work was supported by the Swedish Cancer Society; the Swedish Medical Research Council; Swedish foundation for strategic research; the Medical Faculty, Umeå University; the Royal Swedish Academy of Sciences; the Magn Bergvall Foundation; the Harald Jeanssons Foundation; the Åke Wibergs Foundation; and the National Health and Medical Research Council of Australia (R.G.P.). Gary Doherty was supported by a Trinity College, Cambridge, Internal Graduate Studentship and Research Scholarship and an MRC postdoctoral award. Many thanks to Sven Carlsson and all members of the McMahon lab for help and support. Special thanks to Safa Lucken-Ardjomande for technical assistance regarding molecular cloning and live-cell imaging. Confocal microscopy on migrating cells was performed at the Australian Cancer Research Foundation (ACRF)/Institute for Molecular Bioscience Dynamic Imaging Facility for Cancer Biology, which was established with the support of the ACRF.

REFERENCES

Baldassarre M, Pompeo A, Beznoussenko G, Castaldi C, Cortellino S, McNiven MA, Luini A, Buccione R (2003). Dynamin participates in focal extracellular matrix degradation by invasive cells. Mol Biol Cell 14, 1074–1084.

Block MR, Badowski C, Millon-Fremillon A, Bouvard D, Bouin AP, Faurobert E, Gerber-Scokaert D, Planus E, Albiges-Rizo C (2008). Podosome-type adhesions and focal adhesions, so alike yet so different. Eur J Cell Biol 87, 491–506.

Caswell PT, Vadrevu S, Norman JC (2009). Integrins: masters and slaves of endocytic transport. Nat Rev Mol Cell Biol 10, 843–853.

Chadda R, Howes MT, Plowman SJ, Hancock JF, Parton RG, Mayor S (2007). Cholesterol-sensitive Cdc42 activation regulates actin polymerization for endocytosis via the GEEC pathway. Traffic 8, 702–717.

Claing A, Perry SJ, Achiriloaie M, Walker JK, Albanesi JP, Lefkowitz RJ, Premont RT (2000). Multiple endocytic pathways of G protein-coupled receptors delineated by GIT1 sensitivity. Proc Natl Acad Sci USA 97, 1119–1124.

del Pozo MA, Alderson NB, Kiosses WB, Chiang HH, Anderson RG, Schwartz MA (2004). Integrins regulate Rac targeting by internalization of membrane domains. Science 303, 839–842.

Doherty GJ, McMahon HT (2008). Mediation, modulation, and consequences of membrane-cytoskeleton interactions. Annu Rev Biophys 37, 65–95.

Doherty GJ, McMahon HT (2009). Mechanisms of endocytosis. Annu Rev Biochem 78, 857–902.

Dutartre H, Davoust J, Gorvel JP, Chavrier P (1996). Cytokinesis arrest and redistribution of actin-cytoskeleton regulatory components in cells expressing the Rho GTPase CDC42Hs. J Cell Sci 109, 367–377.

Ezratty EJ, Bertaux C, Marcantonio EE, Gundersen GG (2009). Clathrin mediates integrin endocytosis for focal adhesion disassembly in migrating cells. J Cell Biol 187, 733–747.

Ezratty EJ, Partridge MA, Gundersen GG (2005). Microtubule-induced focal adhesion disassembly is mediated by dynamin and focal adhesion kinase. Nat Cell Biol 7, 581–590.

Gaus K, Le Lay S, Balasubramanian N, Schwartz MA (2006). Integrin-mediated adhesion regulates membrane order. J Cell Biol 174, 725–734.

Gawden-Bone C, Zhou Z, King E, Prescott A, Watts C, Lucocq J (2010). Dendritic cell podosomes are protrusive and invade the extracellular matrix using metalloproteinase MMP-14. J Cell Sci 123, 1427–1437.

Hansen CG, Nichols BJ (2009). Molecular mechanisms of clathrin-independent endocytosis. J Cell Sci 122, 1713–1721.

Hildebrand JD, Taylor JM, Parsons JT (1996). An SH3 domain-containing GTPase-activating protein for Rho and Cdc42 associates with focal adhesion kinase. Mol Cell Biol 16, 3169–3178.

Hoefen RJ, Berk BC (2006). The multifunctional GIT family of proteins. J Cell Sci 119, 1469–1475.

Howes MT *et al.* (2010a). Clathrin-independent carriers form a high capacity endocytic sorting system at the leading edge of migrating cells. J Cell Biol 190, 675–691.

Howes MT, Mayor S, Parton RG (2010b). Molecules, mechanisms, and cellular roles of clathrin-independent endocytosis. Curr Opin Cell Biol 22, 519–527.

Kirkham M, Fujita A, Chadda R, Nixon SJ, Kurzchalia TV, Sharma DK, Pagano RE, Hancock JF, Mayor S, Parton RG (2005). Ultrastructural identification of uncoated caveolin-independent early endocytic vehicles. J Cell Biol 168, 465–476.

Kumari S, Mayor S (2008). ARF1 is directly involved in dynamin-independent endocytosis. Nat Cell Biol 10, 30–41.

Lahuna O, Quellari M, Achard C, Nola S, Meduri G, Navarro C, Vitale N, Borg JP, Misrahi M (2005). Thyrotropin receptor trafficking relies on the hScrib-βPIX-GIT1-ARF6 pathway. EMBO J 24, 1364–1374.

Lee E, De Camilli P (2002). Dynamin at actin tails. Proc Natl Acad Sci USA 99, 161–166.

Lundmark R, Doherty GJ, Howes MT, Cortese K, Vallis Y, Parton RG, McMahon HT (2008). The GTPase-activating protein GRAF1 regulates the CLIC/GEEC endocytic pathway. Curr Biol 18, 1802–1808.

Manabe R, Kovalenko M, Webb DJ, Horwitz AR (2002). GIT1 functions in a motile, multi-molecular signaling complex that regulates protrusive activity and cell migration. J Cell Sci 115, 1497–1510.

Mayor S, Pagano RE (2007). Pathways of clathrin-independent endocytosis. Nat Rev Mol Cell Biol 8, 603–612.

Moreau V, Tatin F, Varon C, Anies G, Savona-Baron C, Genot E (2006). Cdc42-driven podosome formation in endothelial cells. Eur J Cell Biol 85, 319–325.

Nalbant P, Hodgson L, Kraynov V, Toutchkine A, Hahn KM (2004). Activation of endogenous Cdc42 visualized in living cells. Science 305, 1615–1619.

Nobes CD, Hall A (1995). Rho, rac, and cdc42 GTPases regulate the assembly of multimolecular focal complexes associated with actin stress fibers, lamellipodia, and filopodia. Cell 81, 53–62.

Ochoa GC *et al.* (2000). A functional link between dynamin and the actin cytoskeleton at podosomes. J Cell Biol 150, 377–389.

Premont RT, Claing A, Vitale N, Freeman JL, Pitcher JA, Patton WA, Moss J, Vaughan M, Lefkowitz RJ (1998). β_2-Adrenergic receptor regulation by GIT1, a G protein-coupled receptor kinase-associated ADP ribosylation factor GTPase-activating protein. Proc Natl Acad Sci USA 95, 14082–14087.

Sabharanjak S, Sharma P, Parton RG, Mayor S (2002). GPI-anchored proteins are delivered to recycling endosomes via a distinct cdc42-regulated, clathrin-independent pinocytic pathway. Dev Cell 2, 411–423.

Schlunck G, Damke H, Kiosses WB, Rusk N, Symons MH, Waterman-Storer CM, Schmid SL, Schwartz MA (2004). Modulation of Rac localization and function by dynamin. Mol Biol Cell 15, 256–267.

Simpson KJ, Selfors LM, Bui J, Reynolds A, Leake D, Khvorova A, Brugge JS (2008). Identification of genes that regulate epithelial cell migration using an siRNA screening approach. Nat Cell Biol 10, 1027–1038.

Sims TN, Dustin ML (2002). The immunological synapse: integrins take the stage. Immunol Rev 186, 100–117.

Subauste MC, Von Herrath M, Benard V, Chamberlain CE, Chuang TH, Chu K, Bokoch GM, Hahn KM (2000). Rho family proteins modulate rapid apoptosis induced by cytotoxic T lymphocytes and Fas. J Biol Chem 275, 9725–9733.

Taylor JM, Macklem MM, Parsons JT (1999). Cytoskeletal changes induced by GRAF, the GTPase regulator associated with focal adhesion kinase, are mediated by Rho. J Cell Sci 112, 231–242.

Totsukawa G, Yamakita Y, Yamashiro S, Hartshorne DJ, Sasaki Y, Matsumura F (2000). Distinct roles of ROCK (Rho-kinase) and MLCK in spatial regulation of MLC phosphorylation for assembly of stress fibers and focal adhesions in 3T3 fibroblasts. J Cell Biol 150, 797–806.

Wang J, Taba Y, Pang J, Yin G, Yan C, Berk BC (2009). GIT1 mediates VEGF-induced podosome formation in endothelial cells: critical role for PLCγ. Arterioscler Thromb Vasc Biol 29, 202–208.

Wheeler AP, Wells CM, Smith SD, Vega FM, Henderson RB, Tybulewicz VL, Ridley AJ (2006). Rac1 and Rac2 regulate macrophage morphology but are not essential for migration. J Cell Sci 119, 2749–2757.

Winograd-Katz SE, Itzkovitz S, Kam Z, Geiger B (2009). Multiparametric analysis of focal adhesion formation by RNAi-mediated gene knockdown. J Cell Biol 186, 423–436.

Zamir E, Geiger B (2001a). Components of cell-matrix adhesions. J Cell Sci 114, 3577–3579.

Zamir E, Geiger B (2001b). Molecular complexity and dynamics of cell-matrix adhesions. J Cell Sci 114, 3583–3590.

Zhao ZS, Manser E, Loo TH, Lim L (2000). Coupling of PAK-interacting exchange factor PIX to GIT1 promotes focal complex disassembly. Mol Cell Biol 20, 6354–6363.

Supplemental information

The Endocytic Protein GRAF1 is Directed to Cell-Matrix Adhesion Sites and Regulates Cell Spreading

Gary J. Doherty [†1], Monika K. Åhlund [*1], Mark T. Howes [‡], Björn Morén [*], Robert G. Parton [‡], Harvey T. McMahon [†], Richard Lundmark [* §]

[1] *These authors contributed equally to this work*
[*] *Medical Biochemistry and Biophysics, Umeå University, 901 87, Umeå, Sweden*
[†] *MRC Laboratory of Molecular Biology, Hills Road, Cambridge, CB2 0QH, UK*
[‡] *Institute for Molecular Bioscience and Centre for Microscopy and Microanalysis, University of Queensland, Brisbane, Australia*

Supplementary Figure Legends

Figure S1 | GRAF1–positive podosome-like adhesions (PLAs) contain vinculin and actin. (A) Fluorescent micrographs of a HeLa cell expressing high levels of myc-GRAF1 and co-stained for myc, actin (using phalloidin) and vinculin. (B) Bar graph showing the percentage of cells with a protrusive phenotype. Untransfected cells (UTC) and cells expressing myc-GRAF1, myc-GRAF1 R412D (GAP mutant) or myc-GRAF1 BARPH (truncated GRAF1) were analyzed, and cells with thin (<10 μm) and long (>20μm) protrusions were scored as protrusive using Zeiss software. Bars and error bars correspond to mean and SEM calculated from three independent experiments. ($n > 150$, two-tailed Fisher's exact test, $p < 0.001$ <=> ***. (C) Fluorescent micrograph of HeLa cells overexpressing myc-tagged GRAF1 and co-stained for vinculin. (D-G) Fluorescent micrographs of untransfected cells (C), cells transfected with GFP-cdc42-DA and myc-GRAF1 together (D-E) before fixation and staining for the indicated proteins. (F) Fluorescent micrograph of HeLa cells overexpressing GFP-tagged GRAF1 R412D and co-stained for vinculin. Scale bars=10μm.

Figure S2 | Src Y527F induced podosomes contain pFAK, cortactin, vinculin and GRAF1. (A) Single channel confocal micrographs of the merged confocal micrograph presented in Fig. 2D. (B-C) Confocal micrographs of HeLa cell expressing src Y527F and GFP-GRAF1 and co-stained for pFAK (B) or cortactin (C) Scale bars=10μm.

Figure S3 | Drug treatment results in adhesion and actin reorganisation and clustering of CTxB in GRAF1-positive structures. (A-C) Epifluorescent micrographs of HeLa cells treated with vehicle (top panels) or the rhoA kinase inhibitor Y-27632 for 15 minutes, before fixation and staining for actin (A; left panels), the focal adhesion marker vinculin (A; right panels) or endogenous or overexpressed GRAF1 (B-C). (D) Fluorescent micrographs of myc-GRAF1 in Balb/3T3 cells treated with Y-27632 for 15 minutes before fixation and co-staining for myc and vinculin. (E) Fluorescent micrographs of myc-GRAF1-expressing HeLa cells incubated with blebbistatin together with CTxB-Alexa555 for 10 minutes before washing, fixation and co-staining for vinculin. Scale bars=10μm.

Figure S4 | GRAF1–positive carriers originate from, and communicate with, adhesions (A) Representative micrographs from live cell confocal imaging of cell expressing GFP-GRAF1 R412D (GAP mutant) and RFP-paxillin, a marker of integrin-based adhesions. Insets show magnification of the area indicated in the single paxillin channel. Note the recruitment of GRAF1 R412D to the adhesion and subsequent formation of GRAF1 carriers. Time is indicated in seconds. (B) Representative micrographs of area of interest from live cell confocal imaging of a cell treated as in (A). (C) Epifluorescent micrograph of HeLa cells expressing myc-GRAF BARPH (truncated GRAF1 construct) and co-stained for paxillin. Yellow triangles highlights positions were GRAF1 BARPH-positive tubes are associated with sites of focal adhesions. (D-E) Representative micrographs from live cell confocal imaging of cells expressing GFP-GRAF1 BARPH and RFP-paxillin. Note the formation of membrane tubules from adhesions. Scale bars as indicated.

Movie S1 | GRAF1 R412D–positive carriers originates from adhesions. Movie of cell co-transfected with GFP-GRAF1 R412D and RFP-paxillin acquired by live-cell

confocal microscopy. Representative micrographs are shown in Fig S4A. Images were taken every 10 seconds.

Movie S2 | GRAF1 R412D–positive carriers communicates with adhesions. Movie of cell co-transfected with GFP-GRAF1 R412D and RFP-paxillin acquired by live-cell confocal microscopy. Representative micrographs are shown in Fig S4B. Images were taken every 10 seconds.

Movie S3 | GRAF1 BARPH–positive carriers originates from adhesions. Movie of cell co-transfected with GFP-GRAF1 BARPH and RFP-paxillin acquired by live-cell confocal microscopy. Representative micrographs are shown in Fig S4D. Images were taken every 10 seconds.

Movie S4 | GRAF1 BARPH–positive carriers communicates with adhesions. Movie of cell co-transfected with GFP-GRAF1 R412D and RFP-paxillin acquired by live-cell confocal microscopy. Representative micrographs are shown in Fig S4E. Images were taken every 10 seconds.

Movie S5 | Polarised membrane tubulation by GRAF1 is stimulated by Rac1-mediated cell spreading. Movie of cell co-transfected with EGFP-rac1(Q61L) and GRAF1-TagRFP acquired by spinning disk confocal microscopy. Images were taken every 5 seconds.

Supplemental Experimental Procedures

Live cell imaging

For live cell fluorescent microscopy, cells were grown on uncoated MatTek dishes and prior to imaging, the medium was changed to DMEM without phenol red supplemented with 5 % FBS. Cells were then placed in a temperature controlled chamber with 95% air / 5% CO2 and 100 % humidity. Live-cell imaging data were acquired using fully motorized inverted microscopes; (Eclipse TE-2000, Nikon) equipped with a CSU-X1 spinning disk confocal head (UltraVIEW VoX,

Perkin-Elmer, England) using a 60x lens (Plan Apochromat VC Oil DIC N2, Nikon) under control of Volocity 5.0 (Improvision, England) or; (Nikon A1 R Laser Scanning Confocal Microscope) using a 60x lens (Plan Apochromat VC Oil DIC N2, Nikon) under control of the NIS-Elements Microscope Imaging Software. Before acquisition culture medium were switched to phenol free medium. 14-bit digital images were obtained with a cooled EMCCD camera (9100-02, Hamamatsu, Japan). Three 50 mW solid-state lasers (405, 488 and 561 nm; Crystal Laser and Melles Griots) coupled to individual acoustic-optical tunable filters (AOTF, 455/50, 527/55 and 600/50, Chroma) were respectively used as light source to excite tagBFP, EGFP and TagRFP. Single images were taken every 5 or 10 seconds.

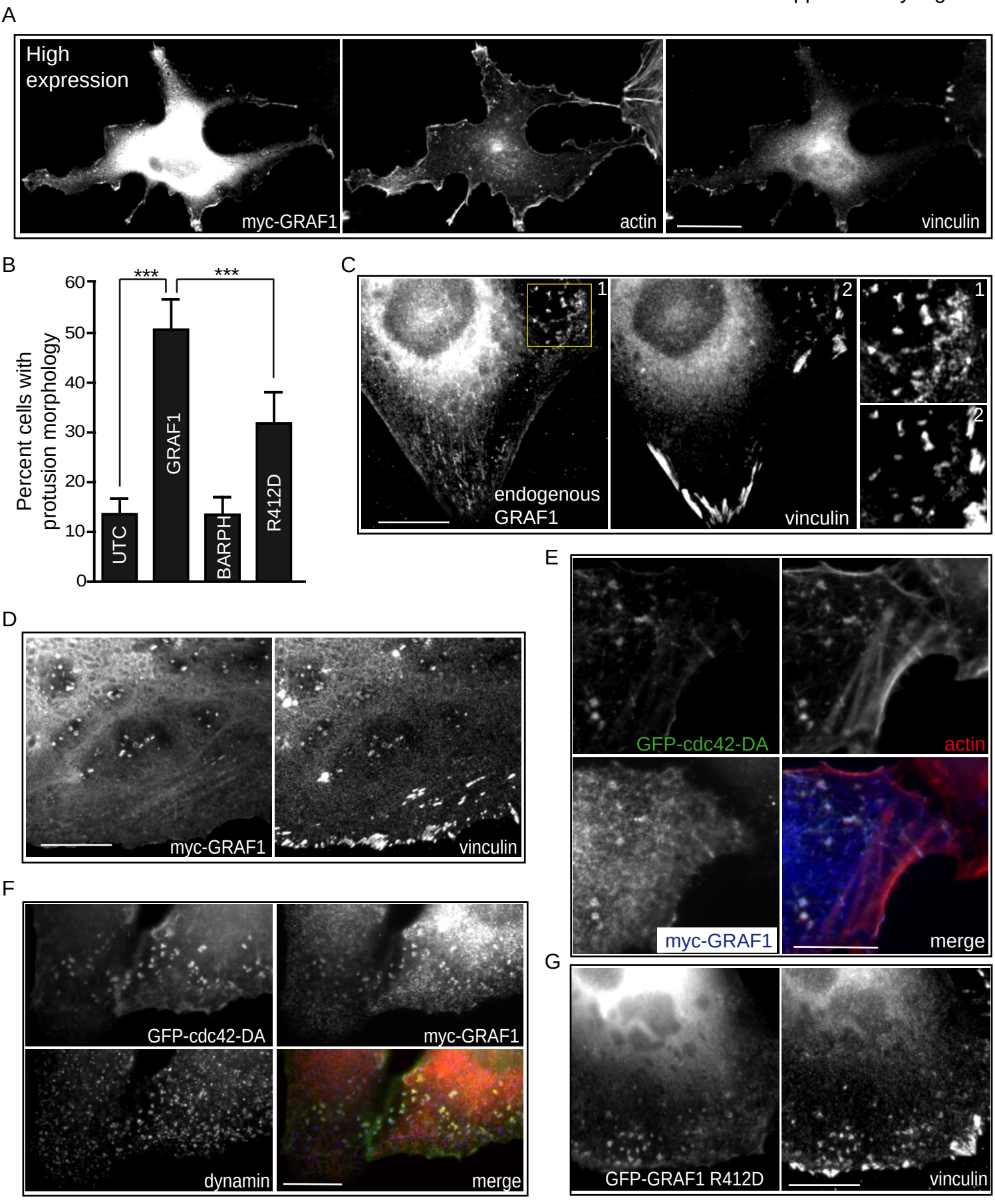
A
High expression
myc-GRAF1
actin
vinculin
B
Percent cells with protusion morphology
60
50
40
30
20
10
0
***
***
UTC
GRAF1
BARPH
R412D
C
1
2
endogenous GRAF1
vinculin
D
myc-GRAF1
vinculin
E
GFP-cdc42-DA
actin
myc-GRAF1
merge
F
GFP-cdc42-DA
myc-GRAF1
dynamin
merge
G
GFP-GRAF1 R412D
vinculin

Supplementary Fig. S2

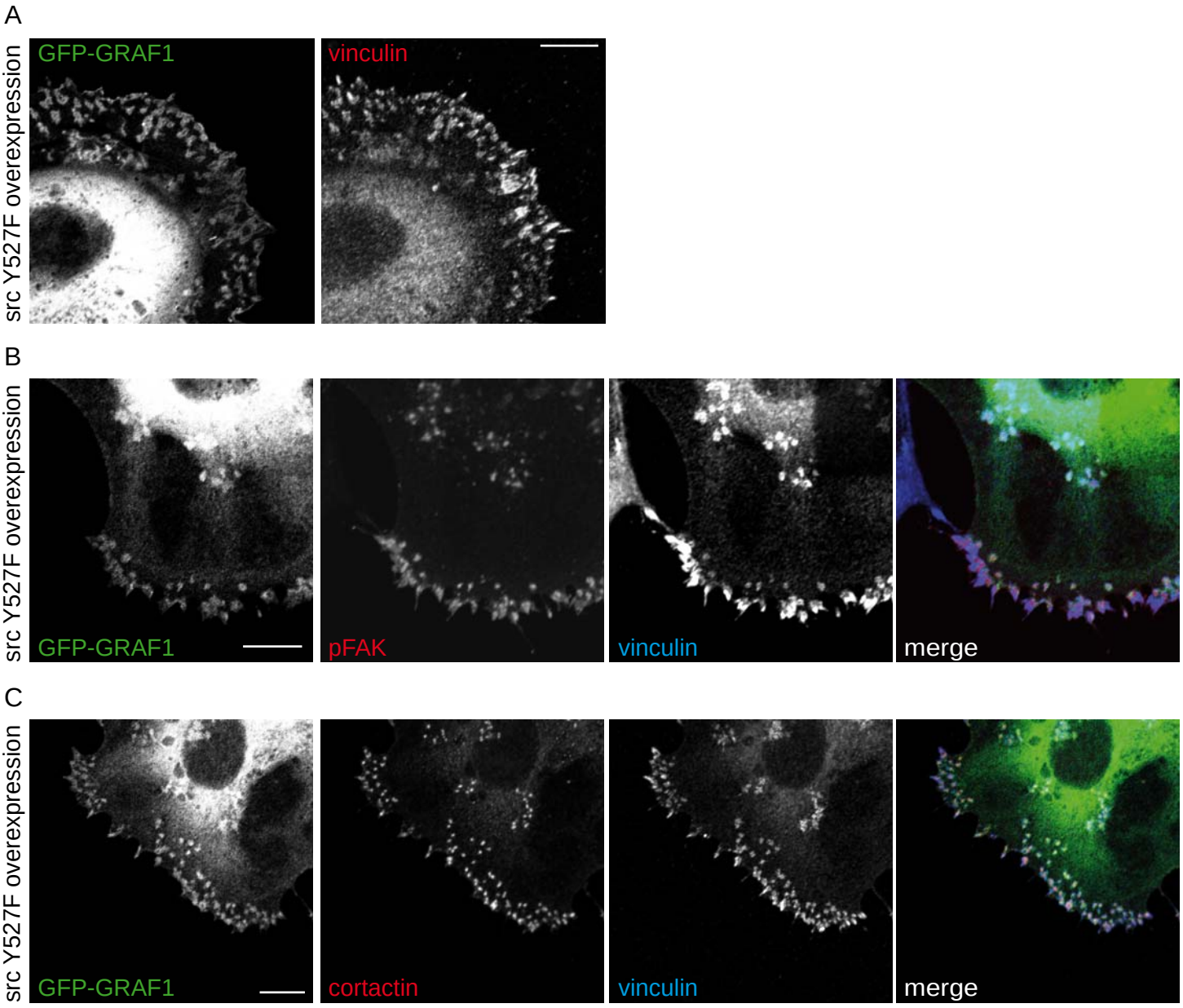

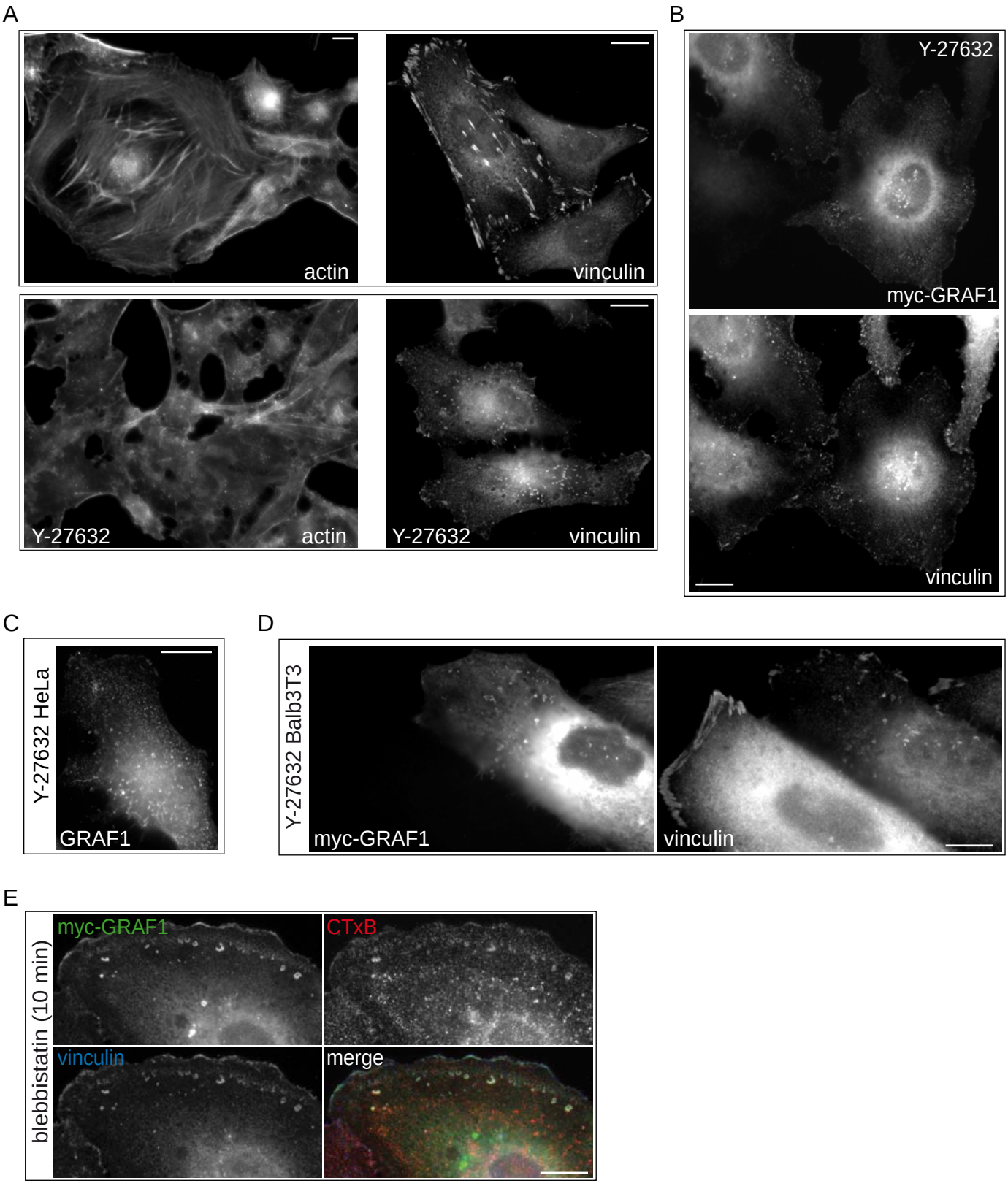
A
actin
vinculin
Y-27632
actin
Y-27632
vinculin
B
Y-27632
myc-GRAF1
vinculin
C
Y-27632 HeLa
GRAF1
D
Y-27632 Balb3T3
myc-GRAF1
vinculin
E
blebbistatin (10 min)
myc-GRAF1
CTxB
vinculin
merge

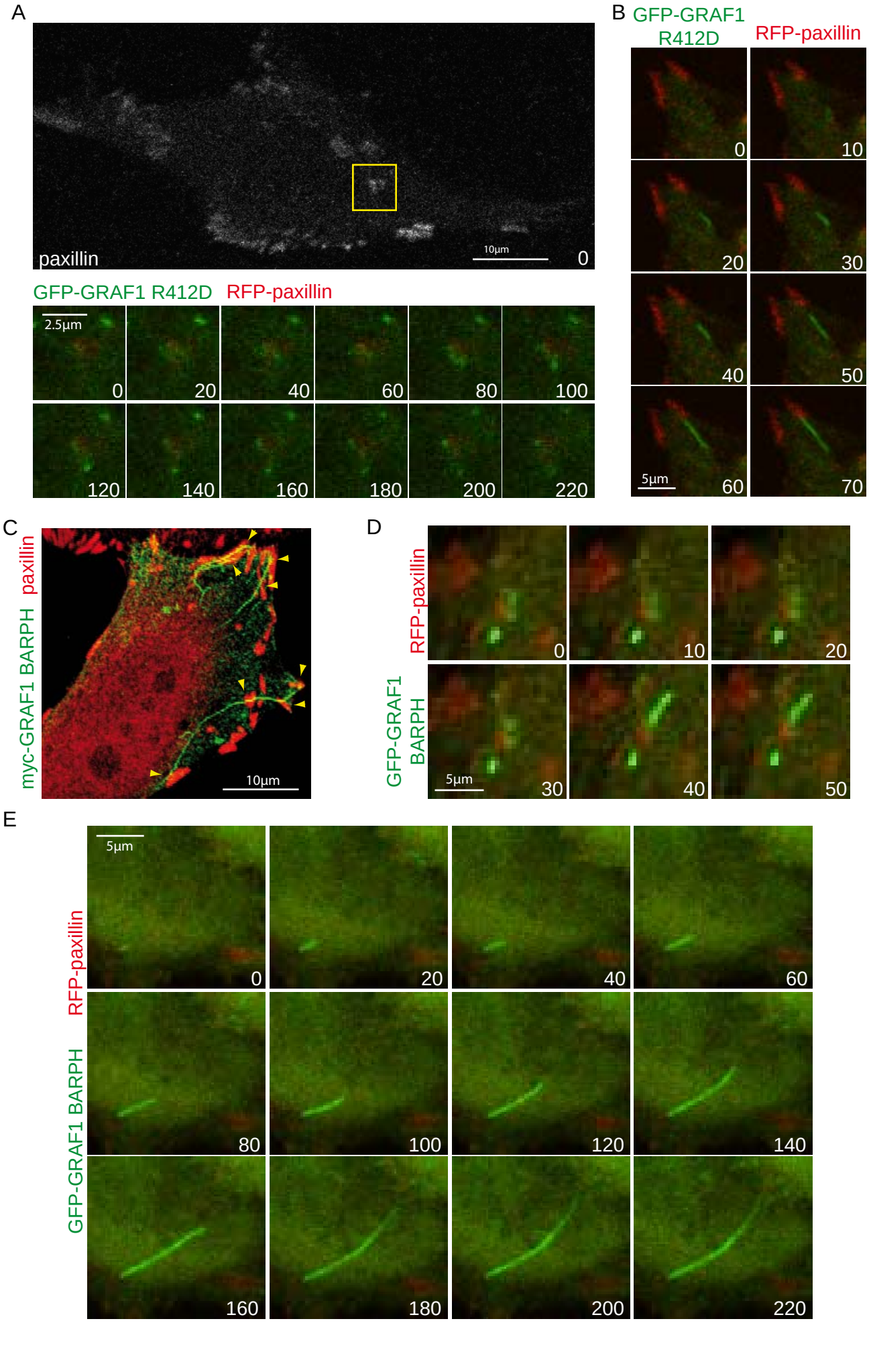
A
paxillin
10μm
0
GFP-GRAF1 R412D
RFP-paxillin
2.5μm
0
20
40
60
80
100
120
140
160
180
200
220
B
GFP-GRAF1 R412D
RFP-paxillin
0
10
20
30
40
50
5μm
60
70
C
myc-GRAF1 BARPH
paxillin
10μm
D
RFP-paxillin
GFP-GRAF1 BARPH
0
10
20
5μm
30
40
50
E
RFP-paxillin
GFP-GRAF1 BARPH
5μm
0
20
40
60
80
100
120
140
160
180
200
220